Cavity modes with optical orbital angular momentum in a metamaterial ring based on transformation optics

H. W. Wu, F. Wang, Y. Q. Dong, F. Z. Shu, K. Zhang, R. W. Peng,* X. Xiong, and Mu Wang

National Laboratory of Solid State Microstructures and School of Physics, Collaborative Innovation, Center of Advanced Microstructures, Nanjing University, Nanjing 210093, China
*rwpeng@nju.edu.cn

Abstract: In this work, we theoretically study the cavity modes with transverse orbital angular momentum in metamaterial ring based on transformation optics. The metamaterial ring is designed to transform the straight trajectory of light into the circulating one by enlarging the azimuthal angle, effectively presenting the modes with transverse orbital angular momentum. The simulation results confirm the theoretical predictions, which state that the transverse orbital angular momentum of the mode not only depends on the frequency of the incident light, but also depends on the transformation scale of the azimuthal angle. Because energy dissipation inevitably reduces the field amplitude of the modes, the confined electromagnetic energy and the quality factor of the modes inside the ring are also studied in order to evaluate the stability of those cavity modes. The results show that the metamaterial ring can effectively confine light with a high quality factor and maintain steady modes with the orbital angular momentum, even if the dimension of the ring is much smaller than the wavelength of the incident light. This technique for exploiting the modes with optical transverse orbital angular momentum may provides a unique platform for applications related to micromanipulation.

OCIS codes: (170.4520) Optical confinement and manipulation; (160.3918) Metamaterials; (260.2110) Electromagnetic optics.

References and links

1. A. Bekshaev, K. Bliokh, and M. Soskin, "Internal flows and energy circulation light beams," J. Opt. **13**(5), 053001 (2011).
2. M. Mansuripur, "Spin and orbital angular momenta of electromagnetic waves in free space," Phys. Rev. A **84**(3), 033838 (2011).
3. J. H. Poynting, "The wave motion of a revolving shaft, and a suggestion as to the angular momentum in a beam of circularly polarized light," Proc. R. Soc. Lond., A Contain. Pap. Math. Phys. Character **82**(557), 560–567 (1909).
4. R. A. Beth, "Mechanical detection and measurement of the angular momentum of light," Phys. Rev. **50**(2), 115–125 (1936).
5. L. Allen, M. W. Beijersbergen, R. J. C. Spreeuw, and J. P. Woerdman, "Orbital angular momentum of light and the transformation of Laguerre-Gaussian laser modes," Phys. Rev. A **45**(11), 8185–8189 (1992).
6. D. G. Grier, "A revolution in optical manipulation," Nature **424**(6950), 810–816 (2003).
7. M. F. Andersen, C. Ryu, P. Cladé, V. Natarajan, A. Vaziri, K. Helmerson, and W. D. Phillips, "Quantized rotation of atoms from photons with orbital angular momentum," Phys. Rev. Lett. **97**(17), 170406 (2006).
8. G. Gibson, J. Courtial, M. Padgett, M. Vasnetsov, V. Pas'ko, S. Barnett, and S. Franke-Arnold, "Free-space information transfer using light beams carrying orbital angular momentum," Opt. Express **12**(22), 5448–5456 (2004).
9. G. Molina-Terriza, J. P. Torres, and L. Torner, "Twisted photons," Nat. Phys. **3**(5), 305–310 (2007).
10. L. Torner, J. Torres, and S. Carrasco, "Digital spiral imaging," Opt. Express **13**(3), 873–881 (2005).
11. K. Dholakia and T. Čižmár, "Shaping the future of manipulation," Nat. Photonics **5**(6), 335–342 (2011).
12. V. Y. Bazhenov, M. V. Vasnetsov, and M. S. Soskin, "Laser beams with screw dislocations in their wavefronts," JETP Lett. **52**(8), 429–431 (1990).
13. N. R. Heckenberg, R. McDuff, C. P. Smith, and A. G. White, "Generation of optical phase singularities by

#246846 Received 27 Jul 2015; revised 20 Nov 2015; accepted 25 Nov 2015; published 4 Dec 2015

computer-generated holograms," Opt. Lett. **17**(3), 221–223 (1992).
14. M. W. Beijersbergen, R. P. C. Coerwinkel, M. Kristensen, and J. P. Woerdman, "Helical-wavefront laser beams produced with a spiral phase plate," Opt. Commun. **112**(5–6), 321–327 (1994).
15. J. E. Curtis and D. G. Grier, "Structure of optical vortices," Phys. Rev. Lett. **90**(13), 133901 (2003).
16. X. Cai, J. Wang, M. J. Strain, B. Johnson-Morris, J. Zhu, M. Sorel, J. L. O'Brien, M. G. Thompson, and S. Yu, "Integrated compact optical vortex beam emitters," Science **338**(6105), 363–366 (2012).
17. L. H. Zhu, M. R. Shao, R. W. Peng, R. H. Fan, X. R. Huang, and M. Wang, "Broadband absorption and efficiency enhancement of an ultra-thin silicon solar cell with a plasmonic fractal," Opt. Express **21**(S3), A313–A323 (2013).
18. D. H. Xu, K. Zhang, M. R. Shao, H. W. Wu, R. H. Fan, R. W. Peng, and M. Wang, "Band modulation and in-plane propagation of surface plasmons in composite nanostructures," Opt. Express **22**(21), 25700–25709 (2014).
19. N. Yu, P. Genevet, M. A. Kats, F. Aieta, J. P. Tetienne, F. Capasso, and Z. Gaburro, "Light propagation with phase discontinuities: generalized laws of reflection and refraction," Science **334**(6054), 333–337 (2011).
20. W. Shu, D. Song, Z. Tang, H. Luo, Y. Ke, X. Lü, S. Wen, and D. Fan, "Generation of optical beams with desirable orbital angular momenta by transformation media," Phys. Rev. A **85**(6), 063840 (2012).
21. Y. F. Yu, Y. H. Fu, X. M. Zhang, A. Q. Liu, T. Bourouina, T. Mei, Z. X. Shen, and D. P. Tsai, "Pure angular momentum generator using a ring resonator," Opt. Express **18**(21), 21651–21662 (2010).
22. N. Grigorenko, N. W. Roberts, M. R. Dickinson, and Y. Zhang, "Nanometric optical tweezers based on nanostructured substrates," Nat. Photonics **2**(6), 365–370 (2008).
23. J. B. Pendry, D. Schurig, and D. R. Smith, "Controlling electromagnetic fields," Science **312**(5781), 1780–1782 (2006).
24. Y. Lai, H. Chen, Z. Q. Zhang, and C. T. Chan, "Complementary media invisibility cloak that cloaks objects at a distance outside the cloaking shell," Phys. Rev. Lett. **102**(9), 093901 (2009).
25. J. Li and J. B. Pendry, "Hiding under the carpet: a new strategy for cloaking," Phys. Rev. Lett. **101**(20), 203901 (2008).
26. J. Z. Zhao, D. L. Wang, R. W. Peng, Q. Hu, and M. Wang, "Watching outside while under a carpet cloak of invisibility," Phys. Rev. E Stat. Nonlin. Soft Matter Phys. **84**(4), 046607 (2011).
27. Y. Lai, J. Ng, H. Chen, D. Han, J. Xiao, Z. Q. Zhang, and C. T. Chan, "Illusion optics: the optical transformation of an object into another object," Phys. Rev. Lett. **102**(25), 253902 (2009).
28. W. X. Jiang, H. F. Ma, Q. Cheng, and T. J. Cui, "Illusion media: Generating virtual objects using realizable metamaterials," Appl. Phys. Lett. **96**(12), 121910 (2010).
29. M. Rahm, D. Schurig, D. A. Roberts, S. A. Cummer, D. R. Smith, and J. B. Pendry, "Design of electromagnetic cloaks and concentrators using form-invariant coordinate transformations of Maxwell's equations," Photon. Nanostruct. Fundam. Appl. **6**(1), 87–95 (2008).
30. H. F. Ma and T. J. Cui, "Three-dimensional broadband and broad-angle transformation-optics lens," Nat. Commun. **1**(8), 124 (2010).
31. X. T. Kong, Z. B. Li, and J. G. Tian, "Mode converter in metal-insulator-metal plasmonic waveguide designed by transformation optics," Opt. Express **21**(8), 9437–9446 (2013).
32. M. Moccia, G. Castaldi, S. Savo, Y. Sato, and V. Galdi, "Independent manipulation of heat and electrical current via bifunctional metamaterials," Phys. Rev. X **4**(2), 021025 (2014).
33. V. Ginis, P. Tassin, C. M. Soukoulis, and I. Veretennicoff, "Confining light in deep subwavelength electromagnetic cavities," Phys. Rev. B **82**(11), 113102 (2010).
34. V. Ginis, P. Tassin, J. Danckaert, C. M. Soukoulis, and I. Veretennicoff, "Creating electromagnetic cavities using transformation optics," New J. Phys. **14**(3), 033007 (2012).
35. S. Chávez-Cerda, M. J. Padgett, I. Allison, G. H. C. New, J. C. Gutierrez-Vega, A. T. O'Neil, I. MacVicar, and J. Courtial, "Holographic generation and orbital angular momentum of high-order Mathieu beams," J. Opt. B Quantum Semiclassical Opt. **4**(2), S52–S57 (2002).
36. A. M. Amaral, E. L. Falcão-Filho, and C. B. de Araújo, "Characterization of topological charge and orbital angular momentum of shaped optical vortices," Opt. Express **22**(24), 30315–30324 (2014).
37. M. V. Berry, "Paraxial beams of spinning light," Proc. SPIE **3487**, 6–11 (1998).
38. M. Borselli, T. Johnson, and O. Painter, "Beyond the Rayleigh scattering limit in high-Q silicon microdisks: theory and experiment," Opt. Express **13**(5), 1515–1530 (2005).

1. Introduction

Optical angular momentum, which can be separated into spin and orbital parts of light, plays a key role in many fundamental and applied researches [1, 2]. It has been recognized that the spin angular momentum along the propagation direction depends on the degree of the circular polarization of a light beam, such findings were revealed in the pioneering works by Poynting [3], and the first experimental evidence was provided by Beth [4]. In 1992, the orbital angular momentum (OAM) of the Laguerre-Gaussian (LG) beam was investigated by Allen *et al.* [5], which launched a new era of angular momentum studies in optics. The research indicated that a beam with a helical wave front, characterized by a phase of $\exp(il\theta)$ (which depends on the azimuthal angle θ and the topological charge l), has a momentum component along the azimuthal direction resulting in an OAM of per photon along the beam axis. Since then,

#246846 Received 27 Jul 2015; revised 20 Nov 2015; accepted 25 Nov 2015; published 4 Dec 2015

optical OAM has grown into a large research field with numerous applications in related to the manipulation of atoms [6] and small particles [7], classical [8] or quantum communication [9], imaging [10], and biophysics [11]. In order to satisfy the needs of various applications, techniques for efficiently generating optical beams carrying OAM are always required. Current schemes for the generation of beams carrying OAM include computer-generated holograms [12, 13], spiral phase plates [14], spatial light modulators [15], and silicon-integrated optical vortex emitters [16]. Recently, with the technological developments in the fabrication of various nanostructures [17, 18], metasurface with special nanostructure have been designed to produce helical beams [19]. Furthermore, the compact metamaterial slab, which can precisely convert the wave front of an arbitrary incident beam into a helical one, has been proposed via transformation optics [20], enabling the output beam to carry the desired OAM.

However, the aforementioned OAM of light that is carried by the helical beam is almost entirely longitudinal; in other words, the OAM is parallel with the propagation direction of the beam. That is because the light beam not only has a momentum component along the azimuthal direction but also has the momentum component along the beam axis. However, transverse OAM of light [21] has not yet been widely studied, as opposed to the longitudinal one. Nevertheless, pure transverse OAM is familiar to us because it appears in classical mechanical system: for example, in the form of a rolling wheel that rotates around an axis perpendicular to the rotational plane. For a massless optical system, it has recently been shown that transverse OAM can be also created using a ring resonator surrounded by a group of nano-rods [21]. Pure transverse OAM of light is especially beneficial in manipulating particles into orbital motion in a two-dimensional plane. This is different from the case of the traditional longitudinal OAM, wherein an additional force is required to balance the radiation force along the propagation direction of the light, owing to the existence of the linear momentum component. However, when the particle size is smaller than the wavelength, it is necessary that the transverse OAM of light induces in subwavelength volume beyond the diffraction limit in order to efficiently trap and manipulate the small particle [22]. Therefore, the investigations on the modes with pure transverse OAM in subwavelength devices are of great significance for manipulation of small particle. In this work, we will theoretically study the cavity modes with transverse OAM in a subwavelength-ring based on transformation optics approach.

As a means of designing complex media that can brings about unprecedented control of electromagnetic fields, transformation optics has attracted much attention recently [23–29]. The basic idea lies in converting a geometric distortion of virtual space into a material distribution (e.g., permittivity and permeability) in real space to guide electromagnetic waves along a predesigned trajectory. This technique has been employed to produce unconventional and novel devices, such as invisibility cloak [23–26], optical illusions device [27, 28], concentrator [29], flattened Luneburg lenses [30] and so on. Furthermore, theoretical insights of transformation optics have been coupled with technological developments in the fabrication of metamaterials in various applications, such as converting the plasmonic modes in a metal-insulator-metal waveguide [31], manipulating the heat and electrical current via bifunctional metamaterials [32], and designing perfect optical cavities [33, 34].

Here, we study the cavity modes with transverse optical OAM in a metamaterial ring via azimuthal coordinate transformation. The metamaterial ring is designed to manipulate the light propagation along the ring by enlarging the azimuthal angle, effectively presenting the modes with transverse orbital angular momentum. First, we theoretically derive the modes with the optical transverse OAM in the metamaterial ring. The theoretical results show that the magnitude of the transverse OAM not only depends on the frequency of the incident light, but also depends on the transformation scale of the azimuthal angle. Next, full-wave simulations are employed to verify the theoretical results by calculating the magnetic field distributions of the different modes in the ring. Finally, because the persistent propagation of the light in the ring is significantly limited by energy dissipation, the confined electromagnetic energy and the quality factor (Q factor) of the modes inside metamaterial ring

#246846 Received 27 Jul 2015; revised 20 Nov 2015; accepted 25 Nov 2015; published 4 Dec 2015

are studied in order to evaluate the stability of the modes with OAM. In this way, the modes with pure transverse OAM in a metamaterial ring could applied to find immediate and interesting applications in small particle manipulation.

2. Theoretical model and analysis

In order to study the modes with the transverse OAM inside a metamaterial ring, we first calculate the electromagnetic field distribution of the system by solving Maxwell's equations. Figure 1(a) shows schematically a device that consists of a hollow cylinder with an inner radius R_1 and an outer radius R_2. The inner region i and the surrounding region iii of the hollow cylinder correspond to free space. However, the interlayer (blue region ii) is filled with the metamaterial. In this paper, we assume that the hollow cylinder extends infinitely along the z-axis. Furthermore, because the system is cylindrically symmetric, cylindrical coordinates are used below.

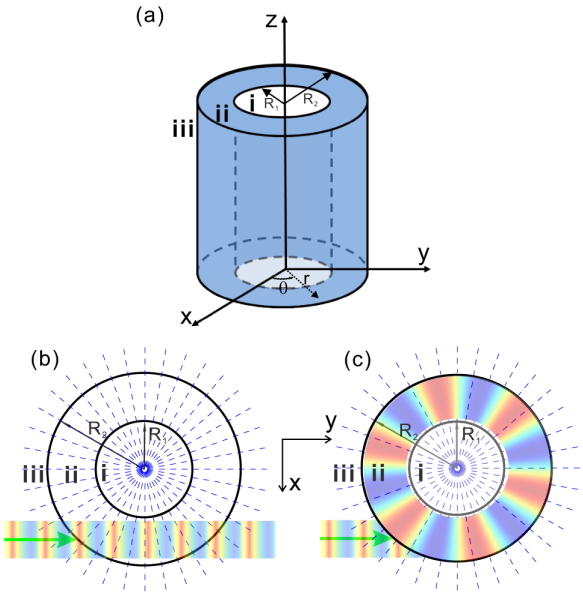

Fig. 1. (a) An infinite hollow cylinder (ii) with inner radius R_1 and outer radius R_2 filled with the metamaterial. The regions (i) and (iii) are free space. Transverse sections of the hollow cylinder for (b) free space and (c) transformation space. The distribution of blue dashed lines indicates that the azimuthal angle of region (ii) in (c) is n times larger than the one in (b). The green solid lines in (b) and (c) represent direction of propagation of incident plane wave.

Without loss of generality, we consider the transverse magnetic (TM) polarization wave, which the magnetic field polarized along the z-axis. The time-harmonic solution can be written as $\mathbf{H}(\Re,t) = H(r,\theta)\mathrm{e}^{-i\omega t}\,\hat{\mathbf{z}}$, where ω is the angular frequency. $\Re$ represents the spatial location in cylindrical coordinates, r and θ represent the radial and azimuthal components, respectively. $\hat{\mathbf{z}}$ is a unit vector in the z direction. Inside regions i and iii, Maxwell's equations can be combined into the free-space Helmholtz's equation for the magnetic field. By using the separation of variables technique, the equations of the radial and angular component can be written as:

$$\begin{cases} \dfrac{1}{H_z(r)} r \dfrac{\partial}{\partial r}\left(r \dfrac{\partial H_z(r)}{\partial r} \right) + k_0^2 r^2 = \chi \\ -\dfrac{1}{H_z(\theta)} \dfrac{\partial^2 H_z(\theta)}{\partial \theta^2} = \chi \end{cases}, \tag{1}$$

#246846 Received 27 Jul 2015; revised 20 Nov 2015; accepted 25 Nov 2015; published 4 Dec 2015

wherein $k_0 = \omega$ / c represents the vacuum wavenumber. χ is an arbitrary constant. Solving the second order differential equations, the magnetic fields are given by considering the finite energy in region (i) and the Sommerfeld radiation condition in region (iii), as follows:

$$H_z^{\mathrm{i}}(r,\theta) = \mathrm{A}\, J_{m_{\nu\mathrm{i}}}(k_0 r)\exp(\mathrm{i}\, m_{\nu\mathrm{i}}\theta), \tag{2}$$

$$H_z^{\mathrm{iii}}(r,\theta) = \mathrm{B}\, H^{(1)}_{m_{\nu\mathrm{iii}}}(k_0 r)\exp(\mathrm{i}\, m_{\nu\mathrm{iii}}\theta), \tag{3}$$

where $J_{m_{\nu\mathrm{i}}}$ and $H^{(1)}_{m_{\nu\mathrm{iii}}}$ are the Bessel and Hankel functions of first kind, respectively, and A, B are arbitrary complex constants. $m_{\nu\mathrm{i}}$ and $m_{\nu\mathrm{iii}}$ are integer constants quantifying the angular momentum of the mode in the regions i and iii, respectively. For the vacuum regions (i and iii), the angular momentum indices satisfy $m_{\nu\mathrm{i}} = m_{\nu\mathrm{iii}} = m$ as a result of the angular component equation independently of the radial coordinate [34].

In order to calculate the field distribution in the region ii by solving Maxwell's equations, we need to obtain the constitutive parameters of the metamaterial that fills in the interlayer. These constitutive parameters can be derived from the coordinate transformation. Figure 1(b) shows the xy-plane of the free space. The materials of regions i, ii, iii are vacuum. The plane wave with TM polarization propagates along the straight line through the lower part of the ring region in the free-space. However, when performing the azimuthal coordinate transformation in region ii, a circulating mode is excited in the interlayer for the same incident plane wave due to enlargement of the azimuthal angle as shown in Fig. 1(c). The azimuthal coordinate transformation from the free space in Fig. 1(b) to the transformation space in Fig. 1(c) for the region ii can be written as

$$\theta' = f(\theta) = n\theta,$$

leaving the radial and z-axes unchanged. Here, n represents the transformation scale of the azimuthal coordinate. Intuitively, once the incident light enters into the transformation region from the lower part of the metamaterial ring, the light is trapped and circulates in the metamaterial ring around the z-axis; then the light is released and recovers the original straight path after n turns. According to transformation optics [23], under a space transformation from the free space to transformation space, the permittivity ε' and permeability μ' in the transformation space can be given by $\varepsilon' = A\varepsilon A^T / \det(A)$, $\mu' = A\mu A^T / \det(A)$, where ε, μ are the permittivity and permeability of the free space, respectively. A is the Jacobian matrix characterized the geometrical variations between the free space and transformation space. Thus, the diagonal elements of the metamaterial parameters matrix can be expressed in cylindrical coordinates as $\varepsilon_r' = n$, $\varepsilon_\theta' = 1/n$, and $\mu_z' = n$. All off-diagonal elements are zero. Inserting the material parameters into Maxwell's equations, the magnetic field in region ii can be written as

$$H_z^{\mathrm{ii}}(r,\theta) = \left(\mathrm{C}\, J_{m_{\nu\mathrm{ii}}}(k_0 r) + \mathrm{D}\, Y_{m_{\nu\mathrm{ii}}}(k_0 r)\right)\exp(\mathrm{i}\, m_{\nu\mathrm{ii}} f(\theta)), \tag{4}$$

where $Y_{m_{\nu\mathrm{ii}}}$ is the Bessel function of the second kind, C and D are the arbitrary complex constants. Similarly, $m_{\nu\mathrm{ii}}$ is the angular momentum index in region ii. For the linear azimuthal transformation $f(\theta) = n\theta$, a single angular momentum index m in the vacuum regions matches a single angular momentum index $m_{\nu\mathrm{ii}}$ in the transformation region ii [34]. Therefore, the index relationship between $m_{\nu\mathrm{ii}}$ and m can be expressed as $m_{\nu\mathrm{ii}} = m / n$.

The field distribution in region ii can be obtained by applying the boundary conditions at $r = \mathrm{R}_1$ and $r = \mathrm{R}_2$. The tangential components of the magnetic field (H_z) and the electric field (E_θ) at the boundaries must be continuous. Accordingly, we have a set of four equations:

#246846 Received 27 Jul 2015; revised 20 Nov 2015; accepted 25 Nov 2015; published 4 Dec 2015

$$\begin{cases} \mathrm{A}\,J_m(k_0\,\mathrm{R}_1) = \mathrm{C}\,J_{m_{v\mathrm{ii}}}(k_0\,\mathrm{R}_1) + \mathrm{D}\,Y_{m_{v\mathrm{ii}}}(k_0\,\mathrm{R}_1) \\ \mathrm{B}\,H_m^{(1)}(k_0\,\mathrm{R}_2) = \mathrm{C}\,J_{m_{v\mathrm{ii}}}(k_0\,\mathrm{R}_2) + \mathrm{D}\,Y_{m_{v\mathrm{ii}}}(k_0\,\mathrm{R}_2) \\ \mathrm{A}\,J'_m(k_0\,\mathrm{R}_1) = n\left(\mathrm{C}\,J'_{m_{v\mathrm{ii}}}(k_0\,\mathrm{R}_1) + \mathrm{D}\,Y'_{m_{v\mathrm{ii}}}(k_0\,\mathrm{R}_1)\right) \\ \mathrm{B}\,H_m^{(1)\prime}(k_0\,\mathrm{R}_2) = n\left(\mathrm{C}\,J'_{m_{v\mathrm{ii}}}(k_0\,\mathrm{R}_2) + \mathrm{D}\,Y'_{m_{v\mathrm{ii}}}(k_0\,\mathrm{R}_2)\right) \end{cases} . \tag{5}$$

Here, the symbol (′) denotes differentiation with respect to the radial coordinate r. The constants A, B, C, and D can be determined by solving the four equations above. The electromagnetic field in each region can be determined by substituting the constants (A, B, C, and D) into Eqs. (2)-(4). Therefore, the azimuthal component of the linear momentum density can be expressed as:

$$P_\theta = \frac{n m_{v\mathrm{ii}}}{\omega r}\mu' \left|\mathrm{C}\,J_{m_{v\mathrm{ii}}}(k_0 r) + \mathrm{D}\,Y_{m_{v\mathrm{ii}}}(k_0 r)\right|^2 , \tag{6}$$

where $\mu' = \mu_0\,\mu_z'$ is the absolute permeability of the transformation medium in region ii. Because the light propagates only in the xy-plane, the linear momentum along the z-direction is zero (i.e., $P_z = 0$). Inserting Eq. (6) into $\boldsymbol{J} = \boldsymbol{r} \times \boldsymbol{P}$, the angular momentum density $\boldsymbol{j}$ carried by the circulating light in region ii can be written as [35, 36]:

$$j_z = \frac{n m_{v\mathrm{ii}}}{\omega}\mu' \left|\mathrm{C}\,J_{m_{v\mathrm{ii}}}(k_0 r) + \mathrm{D}\,Y_{m_{v\mathrm{ii}}}(k_0 r)\right|^2 . \tag{7}$$

The total OAM of the cavity modes in the metamaterial ring is easily obtained by intergrating the angular momentum density over the area of the ring for this case. Equation (7) states that the OAM of light not only depends on the angular frequency ω, but also depends on the transformation scale (n) of the azimuthal coordinate. Furthermore, the orbital angular momentum only exists in the z direction (i.e., $j_x = 0$, $j_y = 0$, $j_z \neq 0$) perpendicular to the momentum due to the circulating light propagated in the xy-plane. It is the reason that the OAM of the modes in the metamaterial ring is transverse one.

3. Numerical results and discussion

In order to present the cavity modes with the transverse optical OAM in the metamaterial ring, we performed full-wave simulations using the commercial software COMSOL MULTIPHYSICS for the TM-polarized incident plane wave. The inner radius and outer radius of the transformed ring region are $\mathrm{R}_1 = 0.5$m and $\mathrm{R}_2 = 1$m, respectively. Without loss of generality, the transformation scale n in the azimuthal coordinate transformation is set as 10. The permittivity and permeability distributions of the metamaterial ring in the Cartesian coordinates are shown in Figs. 2(a) and 2(b), respectively. It is easy to see that the permittivity distribution shows space variation from 0.1 to 10, whereas the permeability remains constant at $\mu_z' = 10$ in the ring region ii.

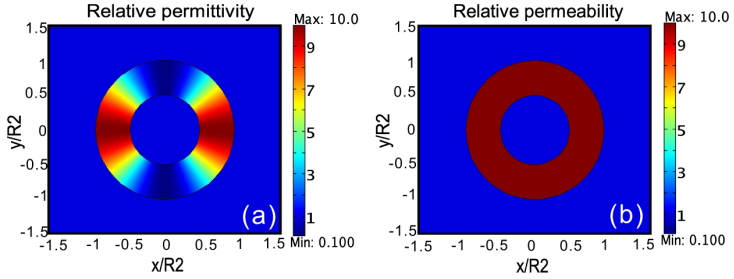

Fig. 2. (a) The permittivity distribution and (b) permeability distribution of the metamaterial ring for $n = 10$.

#246846 Received 27 Jul 2015; revised 20 Nov 2015; accepted 25 Nov 2015; published 4 Dec 2015

In order to determine the frequency of the circulating light that propagates inside the metamaterial ring, we first calculated the normalized extinction cross-section (the extinction cross-section normalizes to the $2R_2$) of the ring as a function of the frequency of the TM-polarized incident light in Fig. 3 for $n = 10$. A series of discrete peaks emerge in the extinction spectrum, corresponding to the frequencies that satisfy the resonance condition of the metamaterial ring. That is to say, the light is effectively confined in the metamaterial ring and the modes with a certain OAM of light is presented at the resonant frequency as a result of constructive interference. When the frequency is non-resonant, the circulating light is not maintained in the ring owing to destructive interference. This property is similar to that of traditional optical micro-ring cavities. However, this mechanism by which stable, circulating light is generated in the metamaterial ring is different from that of the micro-ring cavity. It is well known that circulating light is generated in the cavity owing to the total internal reflection at the interface between the two materials. However, the reason that the metamaterial ring generates circulating light concerns the continuous refraction that results from the anisotropic and inhomogeneous material distribution as Fig. 2. For the sake of simplicity, we only show the five resonant peaks that correspond to the angular momentum indices $m_{vii} = 1$, $m_{vii} = 2$, $m_{vii} = 3$, $m_{vii} = 4$, and $m_{vii} = 5$ for the resonant frequencies $f = 3.3 \times 10^7$ Hz, $f = 4.75 \times 10^7$ Hz, $f = 6.02 \times 10^7$ Hz, $f = 7.085 \times 10^7$ Hz, and $f = 8.06 \times 10^7$ Hz in Fig. 3, respectively.

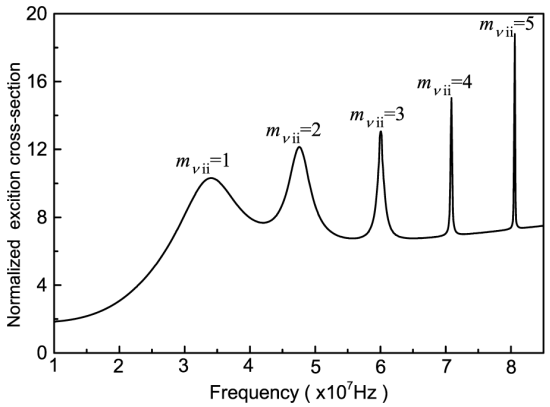

Fig. 3. The normalized extinction cross-section as a function of the frequency of the incident light for the metamaterial ring with inner radius $R_1 = 0.5$m, and outer radius $R_2 = 1$m. The resonant peaks are marked with the angular momentum indices $m_{vii} = 1$, $m_{vii} = 2$, $m_{vii} = 3$, $m_{vii} = 4$, and $m_{vii} = 5$, respectively.

As indicated above, we obtained the resonant frequencies of the circulating light in the metamaterial ring by calculating the normalized extinction cross-section. Next, we show the magnetic field distribution and phase profile of the resonant modes corresponding to the angular momentum indices $m_{vii} = 1$, $m_{vii} = 2$, $m_{vii} = 3$, and $m_{vii} = 4$ for $n = 10$ in Figs. 4(a1)-4(d1) and Figs. 4(a2)-4(d2). Obviously, the field distribution and the phase profile of the Figs. 4(a1) and 4(a2) indicate that the optical path length in the metamaterial ring corresponds to a wavelength of circulating light with a frequency of $f = 3.3 \times 10^7$ Hz. That is to say, the light can stably propagate in the ring and possess the OAM with $m_{vii} = 1$ at this resonant frequency. Particularly, this wavelength is more than nine times larger than the outer radius of the ring for $m_{vii} = 1$. Thus the dimension of the metamaterial ring is subwavelength scale. If the frequency is tuned to $f = 4.75 \times 10^7$ Hz, the wavelength of the resonant light becomes small, two wavelengths of the light can be accommodated in the ring and present the modes with the OAM with $m_{vii} = 2$, as shown in Figs. 4(b1) and 4(b2). Similarly, the field distribution of the sextupole-like and octupole-like are shown in Figs. 4(c1) and 4(d1) for $f = 6.02 \times 10^7$ Hz and $f = 8.06 \times 10^7$ Hz, respectively. In addition, the results can be confirmed from the phase profiles of modes with $m_{vii} = 3$, and $m_{vii} = 4$ in Figs. 4(c2) and 4(d2). In fact, the field

#246846 Received 27 Jul 2015; revised 20 Nov 2015; accepted 25 Nov 2015; published 4 Dec 2015

distribution is similar with the pattern of the m_{vii}-order LG mode in the plane perpendicular to the propagation direction of the beam. It can be find that the circulating light with higher resonant frequency carries larger OAM in the metamaterial ring. Figure 4(e) shows that the total OAM of circulating light in metamaterial ring by integrating the angular momentum density over the area of the ring as a function of the frequency. It is easy to find that the peaks corresponding to the modes possessing the OAM with $m_{vii} = 1$, $m_{vii} = 2$, $m_{vii} = 3$, and $m_{vii} = 4$ locate at the resonant frequencies $f = 3.3 \times 10^7$ Hz, $f = 4.75 \times 10^7$ Hz, $f = 6.02 \times 10^7$ Hz, and $f = 7.085 \times 10^7$ Hz, respectively. Furthermore, the magnitude of peak increases linearly with increase of resonant frequency as show in Fig. 4(e). Physically, when the plane wave with zero OAM comes into the metamaterial ring, the incident wave is transformed to the circulating one with nonzero OAM m_{vii} rotating anticlockwise (or clockwise) in the subwavelength ring. Simultaneously, the metamaterial ring should possess an inverse angular momentum $-m_{vii}$ and rotate clockwise (or anticlockwise) around the z-axis [4, 5, 37]. Thus, the total angular momentum in this system is conservative.

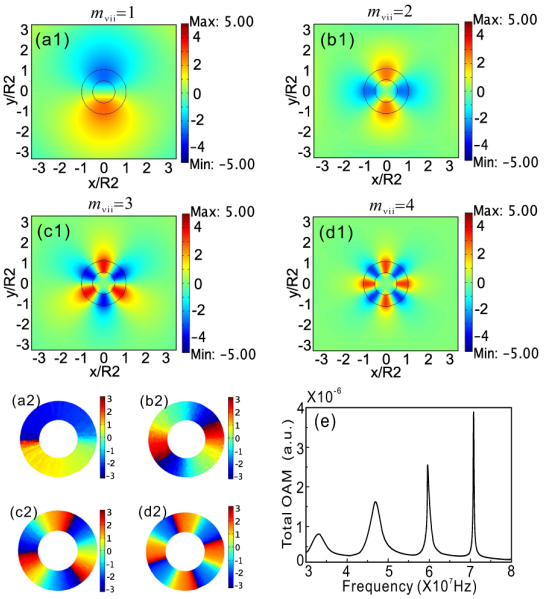

Fig. 4. Magnetic field distributions (a1)-(d1) and field phase profiles (a2)-(d2) of circulating light in the ring with inner radius $R_1 = 0.5$m, and outer radius $R_2 = 1$m correspond to the angular momentum indices $m_{vii} = 1$, $m_{vii} = 2$, $m_{vii} = 3$, and $m_{vii} = 4$ at the resonant frequencies $f = 3.3 \times 10^7$ Hz, $f = 4.75 \times 10^7$ Hz, $f = 6.02 \times 10^7$ Hz, and $f = 7.085 \times 10^7$ Hz for $n = 10$, respectively. The total OAM (e) of circulating light in the metamaterial ring as a function of the frequency.

Next, we also calculated the magnetic field distribution at the frequency $f = 7.085 \times 10^7$ Hz for the transformation scale $n = 10$, 15, 20,and 25 in Fig. 5 in order to discuss how the material of the transformation region ii affects the magnitude of the optical OAM. Here, the frequency and transformation scale of Fig. 5(a) is the same as in Fig. 4(d) as a reference. As we can see in Fig. 5(b), the six wavelengths of light is confined in the ring and the angular momentum index is increased to $m_{vii} = 6$ for $n = 15$. Because the magnetic field in region ii has a factor of $\exp(im_{vii}f(\theta))$ as Eq. (4), which depends on the azimuthal angle $f(\theta) = n\theta$ and the angular momentum index m_{vii}, the angular momentum index is proportionally increased with enlarging the transformation scale n at the same resonant frequency. For example, when we increase the transformation scale from $n = 10$ to $n = 20$, the index is increased from $m_{vii} = 4$ to $m_{vii} = 8$ in Fig. 5(c). Figure 5(d) shows the field distribution with index $m_{vii} = 10$ in the metamaterial ring when the transformation scale is $n = 25$. The physical mechanism behind this phenomenon concerns the fact that the optical path length of the ring is elongated with the

#246846 Received 27 Jul 2015; revised 20 Nov 2015; accepted 25 Nov 2015; published 4 Dec 2015

increasing transformation scale. This leads to the conclusion that magnitude of the OAM depends on the transformation scale n, which is consistent with Eq. (7).

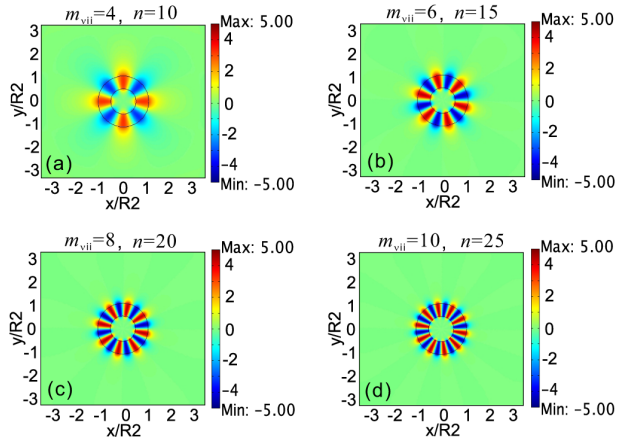

Fig. 5. Magnetic field distributions of the ring with inner radius R_1 = 0.5m, and outer radius R_2 = 1m correspond to the angular momentum indices (a) m_{vii} = 4, (b) m_{vii} = 6, (c) m_{vii} = 8, (d) m_{vii} = 10 at the resonant frequency f = 7.085 × 10^7 Hz for transformation scales n = 10, n = 15, n = 20, and n = 25, respectively.

We have presented the cavity modes with transverse OAM in the metamaterial ring. However, energy dissipation inevitably reduces the field amplitude of the modes with the optical OAM in the metamaterial ring. Thus, the confined electromagnetic energy and the Q factor of the modes are analyzed in order to evaluate the stability of the transverse OAM.

The electromagnetic energy confined inside the metamaterial ring is easily obtained by intergrating the electromagnetic energy density over the area of the ring. Figure 6 shows the confined electromagnetic energy in the metamaterial ring as a function of the frequency for n = 10, n = 15, n = 20. When the transformation scale is set to n = 10, there are three peaks in the energy curve corresponding to the indices m_{vii} = 1, m_{vii} = 2, and m_{vii} = 3 for the frequency span from f = 1 × 10^7 Hz to f = 7 × 10^7 Hz as shown in Fig. 6(a). Obviously, the width and magnitude of the peak corresponding to m_{vii} = 3 are narrower and larger, respectively, compared with the left two peaks. That is to say, more energy of the circulating light propagating in the ring is lossed for the lower resonant frequencies. Generally, the energy dissipation can be attributed to radiation from the resonant modes, scattering related to roughness of the fabricated device, and absorption in the material as the whispering gallery mode in the microdisks [38]. In our system, the energy dissipation mainly results from the radiation losses of the resonant modes. For the metamaterial ring with n = 15, it can be seen that more peaks emerge in the energy curve. Comparing the Figs. 6(a) and 6(b), the peaks corresponding to the angular momentum indices m_{vii} = 1, m_{vii} = 2, and m_{vii} = 3 distinctly redshift. The peaks located at f = 5.67 × 10^7 Hz and f = 6.55 × 10^7 Hz in Fig. 6(b) originate from the redshift of the peaks with the higher frequencies for the case of n = 10 (The peaks are not shown in Fig. 6(a) owing to the fact that the resonant frequencies go beyond the frequency range). Similarly, when we sequentially increase the transformation scale of the azimuthal angle to n = 20 as Fig. 6(c), the peaks continue to red-shift as compared with the peaks presented in Fig. 6(b), and two new peaks emerge in the energy curve. In particular, the peaks with the same index in Figs. 6(a)-6(c) exhibit slight changes. It is not difficult to find that the width and magnitude of the peak become narrow and large, respectively, for the large transformation scale. In other words, in this case the ring maintains particular OAM much better.

#246846 Received 27 Jul 2015; revised 20 Nov 2015; accepted 25 Nov 2015; published 4 Dec 2015

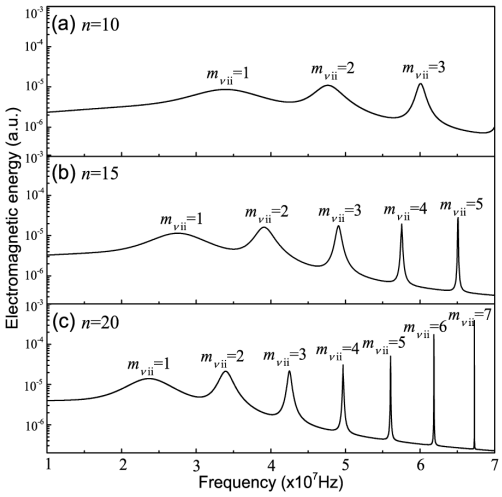

Fig. 6. Electromagnetic energy confined in the metamaterial ring with inner radius R_1 = 0.5m, and outer radius R_2 = 1m as a function of the frequency for the transformation scales (a) n = 10, (b) n = 15, (c) n = 20, respectively.

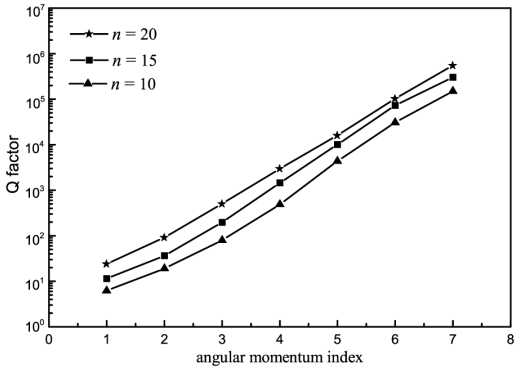

Fig. 7. Quality factor of the modes in the metamaterial ring with inner radius R_1 = 0.5m, and outer radius R_2 = 1m as a function of angular momentum index m_{vii} for transformation scales n = 10 (triangle symbol), n = 15 (square symbol), and n = 20 (pentagram symbol).

In order to straightforwardly evaluate the stability of modes with the optical OAM in the ring, we also calculated the Q factor, which is usually defined as the temporal confinement of the energy normalized to the frequency of oscillation, as a function of the OAM index for n = 10, n = 15, and n = 20 in Fig. 7. The Q factor becomes large with the increasing angular momentum index regardless of the transformation scale n. However, the Q factor for a large transformation scale is obviously higher than the Q factor for the small transformation scale for the same angular momentum index. For the index m_{vii} = 7, although the wavelength of incident light is much larger than the diameter of the ring, the quality factor still exceeds 10^5, regardless of the transformation scale n. The high Q factor indicates that the energy does not dissipate easily when the light propagates in the ring. That is to say, the modes with optical OAM can exist via the circulating light in the metamaterial ring.

4. Conclusions

In this work, we have presented a detailed study on the cavity modes with the transverse optical OAM in a metamaterial ring based on transformation optics. By means of theoretical analysis and numerical simulations, the results show that the transverse OAM of the cavity mode not only depends on the frequency of the incident light but also depends on the

#246846 Received 27 Jul 2015; revised 20 Nov 2015; accepted 25 Nov 2015; published 4 Dec 2015

transformation scale of the azimuthal angle. Furthermore, we have also calculated the Q factor in order to evaluate the stability of the modes with the optical OAM in the metamaterial ring. It is demonstrated that the circulating light can be effectively confined in the ring with a high Q factor, thereby achieves the stable mode with optical OAM, even if the wavelength is larger than the diameter of ring. The technique for exploiting the modes with transverse OAM may have potential applications in the field of micro-manipulation.

Acknowledgments

This work was supported by the Ministry of Science and Technology of China (Grant Nos. 2012CB921502), and the National Natural Science Foundation of China (NSFC) (Grant Nos. 61475070, 11474157, 11574141,11321063, and 91321312).

#246846 Received 27 Jul 2015; revised 20 Nov 2015; accepted 25 Nov 2015; published 4 Dec 2015